HHS Public Access

Author manuscript

Pflugers Arch. Author manuscript; available in PMC 2017 October 01.

Published in final edited form as:

Pflugers Arch. 2016 October ; 468(10): 1651–1661. doi:10.1007/s00424-016-1861-2.

Potassium Channels in the Cx43 Gap Junction Perinexus Modulate Ephaptic Coupling: An Experimental and Modeling Study

Rengasayee Veeraraghavan, Ph.D[1,*], **Joyce Lin, Ph.D**[3], **James P. Keener, Ph.D**[4], **Robert Gourdie, Ph.D**[1,2,*], and **Steven Poelzing, Ph.D**[1,2,*]

[1]Virginia Tech Carilion Research Institute, and Center for Heart and Regenerative Medicine, Virginia Polytechnic University, Roanoke, VA

[2]School of Biomedical Engineering and Sciences, Virginia Polytechnic University, Blacksburg, VA

[3]Department of Mathematics, California Polytechnic State University, San Luis Obispo, CA

[4]Department of Mathematics, University of Utah, Salt Lake City, UT

Abstract

Background—It was recently demonstrated that cardiac sodium channels ($Na_v1.5$) localized at the perinexus, an intercalated disc nanodomain associated with gap junctions (GJ), may contribute to electrical coupling between cardiac myocytes via an ephaptic mechanism. Impairment of ephaptic coupling by acute interstitial edema (AIE)-induced swelling of the perinexus was associated with arrhythmogenic, anisotropic conduction slowing. Given that $K_{ir}2.1$ has also recently been reported to localize at intercalated discs (ID), we hypothesized that $K_{ir}2.1$ channels may reside within the perinexus and that inhibiting them may mitigate arrhythmogenic conduction slowing observed during AIE.

Methods and Results—Using gSTED and STORM super-resolution microscopy, we indeed find that a significant proportion of $K_{ir}2.1$ channels reside within the perinexus. Moreover, whereas $Na_v1.5$ inhibition during AIE exacerbated arrhythmogenic conduction slowing, inhibiting $K_{ir}2.1$ channels during AIE preferentially increased transverse conduction velocity - decreasing anisotropy and ameliorating arrhythmia risk compared to AIE alone. Comparison of our results with a nanodomain computer model identified enrichment of both $Na_v1.5$ and $K_{ir}2.1$ at intercalated discs as key factors underlying the experimental observations.

Conclusions—We demonstrate that $K_{ir}2.1$ channels are localized within the perinexus alongside $Na_v1.5$ channels. Further, targeting $K_{ir}2.1$ modulates intercellular coupling between cardiac

Address correspondence to: Steven Poelzing, Ph.D., Virginia Tech Carilion Research Institute, 2 Riverside Circle, Roanoke, VA 24016, TEL: (540) 526-2108, FAX: (540) 985-3373, poelzing@vtc.vt.edu; James Keener, Ph.D., Department of Mathematics, University of Utah, 155 South 1400 East, Salt Lake City, UT, 84112, USA., TEL: (801) 581-6089, FAX: (801) 581-4148, keener@math.utah.edu; Robert G. Gourdie, Ph.D., Virginia Tech Carilion Research Institute, 2 Riverside Circle, Roanoke, VA 24016, TEL: (540) 526-2095, FAX: (540) 985-3373, gourdier@vtc.vt.edu; Rengasayee Veeraraghavan, Ph.D., Virginia Tech Carilion Research Institute, 2 Riverside Circle, Roanoke, VA 24016, TEL: (540) 526-2130, FAX: (540) 985-3373, saiv@vt.edu.
*Co-corresponding authors

Conflicts of Interest: None.

Disclosures: None.

myocytes, anisotropy of conduction and arrhythmia propensity in a manner consistent with a role for ephaptic coupling in cardiac conduction.

Introduction

Cardiac conduction has classically been viewed as an electrotonic process occurring by means of direct ionic current flow from cell to cell via gap junctions (GJ).(11) Under this view, direction-dependent changes in action potential propagation in the heart were attributed to intercellular communication - in turn determined by GJ, myocyte geometry and tissue architecture.(11) On the other hand, ionic currents, principally the cardiac sodium current (I_{Na}), were thought to be responsible for membrane excitability and thereby, direction-independent changes in cardiac conduction.

The inward-rectifying potassium current (I_{K1}), with its role in setting resting membrane potential, was thought to indirectly affect excitability by modulating the availability of cardiac sodium channels ($Na_v1.5$). However, evidence has emerged to support a more direct role for potassium channels in determining membrane excitability and cardiac conduction (14, 33, 35) Specifically, it has been demonstrated previously that inhibiting the inward-rectifier K^+ channels ($K_{ir}2.1$) in intact ventricles resulted in faster conduction, suggesting that the inward-rectifier K^+ current (I_{K1}) may oppose early depolarization driven by the sodium current (I_{Na})(35).

The understanding of cardiac conduction may be undergoing a paradigm shift. Evidence is mounting that ion channels localized at the intercalated disc, actively participate in intercellular coupling.(13, 17, 21) One leading hypothesis envisions ion channels mediating intercellular communication through transient accumulation or depletion of ions within restricted extracellular clefts located within the intercalated disc. In this non-canonical ephaptic model of conduction, intercalated disc-localized ion channels function as part of cell-to-cell junctions. Thus, targeted modulation of these channels should preferentially impact transverse conduction, since the activation wavefront encounters more cell-to-cell junctions per unit distance traveling transverse to the fiber direction than along it. Indeed, in recent work, we provided experimental evidence that $Na_v1.5$ channels, localized at the perinexus adjacent GJ, play a major role in cell-to-cell propagation in the heart via ephaptic mechanisms.(6, 34) We also demonstrated that our observations across multiple experimental conditions were well predicted by a micro-domain computer model incorporating ephaptic coupling as well as preferential localization of sodium channels to the intercalated disc. Given that $K_{ir}2.1$ channels have been reported to localize at the intercalated disc,(20) we hypothesized that $K_{ir}2.1$ channels co-reside with $Na_v1.5$ in the perinexus and modulate ephaptic coupling and thereby, anisotropic conduction in the ventricular myocardium. Here we added a further layer of refinement to our computer model in the form of preferential localization of $K_{ir}2.1$ to the intercalated disc and compared results across six different experimental conditions.

Methods

The investigation was conducted in conformation with the *Guide for the Care and Use of Laboratory Animals* published by the US National Institutes of Health (NIH Publication No. 85-23, revised 1996). All animal study protocols were approved by Institutional Animal Care and Use Committee (IACUC) at the Virginia Polytechnic University.

Animals

Neonatal myocyte cultures were prepared as previously described using myocytes isolated from ventricles of 2-day-old Sprague-Dawley rats.(24) Additionally, ventricles were isolated as previously described from adult male guinea pigs (800-1000g) and either frozen for cryosectioning or perfused as Langendorff preparations.(34-36)

Neonatal Rat Ventricular Myocyte (NRVM) cultures

Freshly isolated ventricles were placed in cold HBSS, minced and enzymatically dissociated into individual myocytes at 37°C. Myocytes were enriched by centrifugation on a Percoll density gradient 1.08/1.06 and plated in M199/EBSS, 5 % NCS, 10 % HS, and antibiotics onto gelatin-coated coverslips. After attachment at 37°C / 5% CO2, cells were washed in DPBS Ca^{2+}/Mg^{2+} and maintained in culture for 5 days with maintenance media added every 2 days.

Immunolabeling

Cells and tissue sections were fixed in 2% paraformaldehyde at room temperature for 5 minutes and immunofluorescent staining was performed as previously described.(23, 24) Briefly, Samples were labeled using mouse anti-Cx43 (Millipore MAB3067, 1:100), rabbit anti-$Na_v1.5$ (kindly provided by Dr. Peter Mohler, 1:100) and rabbit anti-$K_{ir}2.1$ (Alomone Labs, APC-026, 1:100) antibodies. Goat anti-mouse AlexaFluor 546 (1:4000) and goat anti-rabbit AlexaFluor 488 (1:4000) secondary antibodies were used for confocal microscopy while goat anti-rabbit Alexa 647 (1:4000) and donkey anti-mouse Cy3b (1:100) secondary antibodies were used for super-resolution **ST**ochastic **O**ptical **R**econstruction **M**icroscopy (STORM). Goat anti-rabbit Chromeo 505 (1:100) and anti-mouse biotin (1:200) followed by streptavidin-conjugated Horizon V500 (1:100) secondary antibodies were used for **g**ated **ST**imulated **E**mission **D**epletion (gSTED) microscopy.

Confocal, gSTED & STORM Microscopy

Confocal and gSTED Imaging were performed using a TCS SP8 laser scanning confocal microscope equipped with gSTED modules, a Plan Apochromat 63×/1.4 numerical aperture oil immersion objective, Leica HyD hybrid detectors and a 592nm STED depletion laser (Leica, Buffalo Grove, IL). Sequential imaging of individual fluorophores was performed with the excitation wavelength switched between frames. Also, gSTED and confocal imaging were performed sequentially and gSTED images were deconvolved using Huygens STED deconvolution software (Scientific Volume Imaging, Hilversum, The Netherlands). A maximum lateral ‘full width at half maximum’ resolution approaching 22 nm was achieved using gSTED(2, 25).

gSTED images were analyzed using custom Matlab software (Mathworks, Natick, MA) as previously described.(34) Briefly, a nearest-neighbor algorithm was used to identify clusters in each color channel and the geometric properties of the identified clusters were then calculated. The edge-to-edge distance from each cluster of a given species to the closest cluster of the other species was calculated. In addition, the perinexal region (defined as extending 200 nm from the edge of the Cx43 signal(24)) was demarcated for each Cx43 cluster and $Na_v1.5$ and $K_{ir}2.1$ clusters present within that region were identified.

STORM microscopy was performed using a Vutara 350 microscope equipped with biplane 3D detection and fast-sCMOS imaging achieving 20 nm XY and 50 nm Z resolution. The 3-dimensional location of each identified fluorophore in the STORM dataset was analyzed using the recently published STORM-based Relative Localization Analysis (STORM-RLA) technique.(32) Briefly, clusters of molecules were defined based on their spatial densities, (31) and the interactions between clusters of different types were quantified by the spatial extent of overlap, if any, and distance of closest apposition.

Guinea Pig Langendorff Preparations

Ventricles were extracted from adult male guinea pigs (800-1000g) anaesthetized with 30 mg/kg sodium pentobarbital (Nembutal) IP and perfused (at 40-55 mm Hg) as Langendorff preparations with oxygenated Tyrode's solution (containing, in mM, $CaCl_2$ 1.25, NaCl 140, KCl 4.5, dextrose 5.5, $MgCl_2$ 0.7, HEPES 10; NaOH 5.5mM pH 7.41) at 37°C as previously described(22, 35). Control Tyrode's solution was perfused for 35 minutes in all optical mapping experiments. Ventricles were paced from the anterior left ventricular (LV) epicardium (midapicobasal) at a basic cycle length of 300 ms with 1 ms pulses at 1.5-times the pacing threshold as described previously.(35)

Acute interstitial edema (AIE) was induced by mannitol (26.1 g/l / 143.2 mOsm) perfusion while the sodium current (I_{Na}) and the inward-rectifier potassium current (I_{K1}) were respectively inhibited by flecainide (Flec; 0.5 μM) and barium chloride ($BaCl_2$; 10 μM). Measurements were made 10 minutes following the start of each intervention or combination of interventions.

Electrocardiography

Volume conducted electrocardiograms (ECGs) were collected at 1kHz as previously described. (34-36) Ventricular tachycardia was defined as three or more un-paced consecutive heartbeats with a cycle length shorter than 130 ms.

Optical Mapping

Optical voltage mapping was performed using the voltage sensitive dye di-4-ANEPPS (15 μM) to quantify conduction velocity (CV) and anisotropy (AR; the ratio of longitudinal to transverse CV), as previously described.(22, 35) Briefly, ventricles stained with di-4-ANEPPS by direct coronary perfusion for 10 minutes were excited by LED light sources fitted with 510±5 nm filters (Chroma, Rockingham, VT). A SciMedia MiCam02 HS CCD camera (SciMedia, Irvine CA) in a tandem lens configuration was used to record fluoresced light filtered through a 610 nm LP filter (Newport, Irvine, CA). The system is capable of

resolving membrane potential changes as small as 2 mV from 90 × 60 sites (16.5 × 12 mm) simultaneously at 1 kHz temporal resolution.

Motion was reduced with 7.5 mM 2,3-butanedione monoxime (BDM) combined with mechanical stabilization of the anterior epicardium against the front wall of the perfusion chamber. Activation time was defined as the time of the maximum first derivative of the action potential.(7)

Mathematical modeling

Conduction was simulated in a sheet of 3-dimensional myocytes using a previously described nanodomain model.(17, 34) Briefly, cardiac myocytes were represented as rectangular prisms with corner inclusions and were organized into a sheet to simulate anisotropic propagation. Cells were coupled via GJ located at the ends of myocytes. While the extracellular space was finely discretized, the intracellular space was discretized by linearly interpolating triangular elements with a node placed in each corner of each cell. Parameter values for the experimental conditions are summarized in Table 1.

Both longitudinal and transverse conduction were examined in the model while varying lateral and junctional extracellular conductances ($\bar{\sigma}_e$ and $\bar{\sigma}_j$), sodium and potassium peak conductances (g_{Na} and g_K), and cellular distribution of sodium and potassium channels. For a detailed description of the nanodomain model, the reader is referred to our previous articles.(17, 34)

Statistical analysis

Statistical analysis of data was performed as previously reported.(34, 36) Briefly, parametric data were analyzed using a single factor ANOVA or 2-tailed Student's t-test with Šidák correction for paired and unpaired data. A Fisher's exact test was used to test for significance in nominal data. A $p<0.05$ was considered statistically significant. All data are reported as mean ± standard error unless otherwise noted.

Results

Inward-rectifier Potassium Channel Distribution

We performed confocal microscopy on sections of guinea pig ventricle in order to assess the cellular distribution of $K_{ir}2.1$ protein. Immunosignals corresponding to $K_{ir}2.1$ (red) co-distributed at the intercalated discs along with immunosignals corresponding to Cx43 (green; figure 1) and the confocal co-localization index between the two signals was measured at 44 ± 6%. However, at higher magnifications, the two proteins appeared adjacent to each other rather than overlapping, i.e., the two signals were not directly colocalized (figure 1, insets). This finding closely parallels our recent reports on $Na_v1.5$ and Cx43: Specifically, using super-resolution gSTED(34) and STORM(32) imaging, $Na_v1.5$ was found to be preferentially enriched within the non-junctional perinexal nanodomain surrounding Cx43 GJ in adult guinea pig ventricles.

Here, we performed STORM super-resolution imaging to quantitatively assess $K_{ir}2.1$ localization relative to Cx43 in sections of adult guinea pig ventricles. A representative

STORM image in figure 2A shows individual fluorophore molecules corresponding to Cx43 (green) and $K_{ir}2.1$ (red) depicted as colored spheres, and both proteins can be observed in high density at the intercalated disc. A higher magnification view in figure 2B reveals some areas where Cx43 and $K_{ir}2.1$ exist in mixed populations; however, most areas of high Cx43 density have dense populations of $K_{ir}2.1$ located adjacent to them rather than the proteins existing in a mixed cluster. Quantitative assessment by STORM-RLA revealed that only 10.9% of Cx43 clusters (i.e. presumptive GJ) demonstrated direct overlap with $K_{ir}2.1$ clusters (figure 2C) accounting for 21.1% of intercalated disc-localized $K_{ir}2.1$ clusters (figure 2D). Importantly, an additional 28.8% of Cx43 clusters had $K_{ir}2.1$ located less than 200 nm away from the GJ edge (figure 2C) -the previously reported extent of the perinexus - accounting for 31.4% of total $K_{ir}2.1$ clusters (figure 2D). Overall, the median distance from Cx43 clusters to the nearest $K_{ir}2.1$ cluster was measured at 341 ± 13 nm. Thus, a sub-population of intercalated disc-localized $K_{ir}2.1$ exists within juxta-GJ membranes where we previously also identified a high density of $Na_v1.5$.

In order to determine whether juxta-GJ enrichment of $Na_v1.5$ and $K_{ir}2.1$ varied with age and/or species, we analyzed super-resolution gSTED images of neonatal rat ventricular myocytes (NRVMs). $K_{ir}2.1$ clusters were located at a median distance of 450 ± 58 nm from the nearest Cx43 clusters (figure 4). Importantly, only 5% of Cx43 GJs had overlapping $K_{ir}2.1$ signal whereas 40% had $K_{ir}2.1$ located within 200 nm of the cluster/plaque edge, i.e. within the perinexus. While only 3% of $K_{ir}2.1$ clusters demonstrated direct overlap with GJ, 12.5% were located within perinexal regions surrounding GJs. These results are consistent with the aforementioned results obtained using STORM in adult guinea pig ventricles.

Given the close association between Cx43 and $Na_V1.5$ in adult guinea pig ventricles, we next examined these two proteins in NRVMs. The median edge-to-edge distance between Cx43 and $Na_v1.5$ clusters was measured from gSTED images at 129 ± 16 nm (figure 3) in NRVM. While only 9% of Cx43 clusters demonstrated direct overlap with $Na_v1.5$ clusters, 53% had $Na_v1.5$ cluster(s) within 200 nm of their edge, i.e. within the perinexus. Likewise, 9% of all $Na_v1.5$ clusters demonstrated direct GJ overlap, whereas 37% were located within perinexal regions. These results in NRVMs are consistent with our recently published results obtained from adult guinea pig myocardium.(32, 34) Notably, the difference in median distance from Cx43 between $Na_V1.5$ and $K_{ir}2.1$ suggests a difference in the distribution of these channels between juxta-GJ membranes and the rest of the ID; however, a high proportion of Cx43 GJ had both channels located within their perinexi.

In summary, we demonstrate in two different preparations that significant sub-populations of intercalated disc-localized $Na_V1.5$ and $K_{ir}2.1$ exist in close proximity to Cx43 GJs.

Conduction Dependence on AIE, I_{Na} and I_{K1} - Experiments

We previously demonstrated that I_{K1} inhibition by $BaCl_2$ can increase conduction velocity (CV)(35). Additionally, we demonstrated that acute interstitial edema (AIE) was associated with a selective increase in intermembrane spacing within the perinexus(34), as well as preferential transverse conduction slowing (34, 36). Therefore, we sought to assess whether I_{K1} inhibition could mitigate conduction slowing during AIE. To this end, we performed optical mapping on Langendorff-perfused guinea pig ventricles and quantified conduction

velocity. Under control conditions, longitudinal (CV_L) and transverse (CV_T) conduction velocities were measured at 55.1 ± 1.4 and 19.6 ± 0.1 cm/s respectively, resulting in an anisotropic ratio (AR) of 2.8 ± 0.1 (figure 5A, F). AIE slowed conduction, particularly in the transverse direction (figure 5B, F), as we previously reported.(34, 36) Importantly, partial I_{K1} inhibition during AIE preferentially increased CV_T more than CV_L and decreased AR relative to AIE alone (figure 5C, F). These data suggest that partial I_{K1} inhibition mitigates anisotropic conduction slowing during AIE. The increase in CV elicited by I_{K1} inhibition during AIE, taken together with our previously published time control data,(34) also demonstrate that conduction slowing observed in our experiments is not simply a result of run-down of the preparation.

As in our previous study, partial I_{Na} inhibition (0.5 μM) during AIE preferentially slowed transverse conduction and increased anisotropy (AR) relative to AIE alone (figure 5D, F). In this setting of AIE and partial I_{Na} inhibition, I_{K1} inhibition did not measurably alter CV (figure 5E, F).

Conduction Dependence on AIE, I_{Na} and I_{K1} - Modeling

Next we compared these experimental observations against two computer models that we previously described(17, 34) - a *uniform model* where ion channels are uniformly distributed around the myocyte membrane and a *polarized model* incorporating enrichment of $Na_v1.5$ and $K_{ir}2.1$ enrichment at the intercalated disc. The *polarized model* presented here was modified to include subcellular $K_{ir}2.1$ localization in addition to subcellular $Na_v1.5$ localization, which was included in our previously published model.(34) For all values of potassium channel conductance (g_K) tested, the *uniform model* predicted that increasing extracellular conductivity would increase CV_L as evidenced by the upward shift of the CV_L curves in Figure 6 (top). Once again, the *uniform model* predicted that CV_T is insensitive to increases in extracellular conductance (σ_e; figure 6, top). In other words, the *uniform model* predicted a preferential increase in CV_L during AIE and thus, did not match experimental observations.

In contrast, increasing sodium *and* potassium current density within the intercalated disc with the *polarized model* predicted that AIE should decrease both CV_L and CV_T, as evidenced by the downward shift in the CV_L and CV_T curves in Figure 6 (bottom). Additionally, the *polarized model* correctly anticipated an increase in AR during AIE secondary to the preferential slowing of CV_T over CV_L. Under these conditions, lowering g_K in the *polarized model* to simulate I_{K1} inhibition reduced AR relative to simulated AIE alone. Thus, the polarized model was consistent with both experimental AIE and I_{K1} inhibition during AIE.

We next assessed the relationship between CV, σ_e and I_{Na}, at nominal and reduced g_K. The *uniform model* predicted that with nominal g_K (figure 7, top, black lines) increasing g_{Na} should modestly increase AR by preferentially increasing CV_L over CV_T (figure 7, top panels). Decreasing g_K in the *uniform model* (figure 7, top, red lines) decreased the AR at all g_{Na} and σ_e tested, once again by preferentially affecting CV_L over CV_T. Thus, the *uniform model*'s predictions contrasted with experimental results where CV_T was more sensitive than CV_L to g_{Na} and g_K. Further, the *uniform model* incorrectly predicted a direct relationship

between AR and g_{Na} under nominal g_K and an inverse relationship between AR and g_{Na} when g_K is reduced. In experiments, AR and g_{Na} were inversely related during nominal g_K as well as when g_K was reduced.

The *polarized model* also predicted that, with nominal g_K, increasing g_{Na} should preferentially increase CV_T over CV_L, resulting in decreased AR for all values of σ_e (figure 7, bottom, black lines), which is consistent with our experimental observations. Additionally, the highest AR was observed in the *polarized model* when σ_e was greatest and g_{Na} lowest. These predictions were all consistent with experimental data. Reducing g_K in the *polarized model* (figure 7, bottom, red lines) preferentially increased CV_T over CV_L, thereby, lowering AR. This was particularly the case when σ_e was nominal and occurred to a lesser extent when σ_e was increased. In other words, the *polarized model* predicts that reducing g_K during AIE should significantly reduce AR when g_{Na} is nominal (100%), and this is consistent with experimental results. However, when g_{Na} is reduced, reducing g_K has a much lower impact on AR, and in experiments, we found that I_{K1} inhibition during AIE + I_{Na} inhibition did not significantly alter AR. This is because I_{K1} inhibition during AIE + I_{Na} inhibition was incapable of significantly increasing CV_L or CV_T, just as the *polarized model* anticipated.

Arrhythmia Incidence

In our previous study, we demonstrated that incidence of spontaneous VTs (polymorphic tachyarrhythmias persisting for at least 1 minute) was elevated during AIE (4/11 preparations; representative traces in figure 8) compared to control (0/12 preparations) and that it was further increased by the combination of AIE and I_{Na} inhibition (7/9 preparations).(34) While we determined that partial I_{K1} inhibition during AIE lowered VT incidence (1/8 preparations, p = ns vs. control), all arrhythmias quantified from the bath ECGs were polymorphic and persisted for more than 1 minute. Therefore, partial I_{K1} inhibition decreased arrhythmia propensity without observably altering the type of arrhythmias, as we did not observe any change in the arrhythmia morphology or ectopic beat formations for examples. These data are consistent with the relationship between altering cardiac conduction and arrhythmia propensity.

Discussion

We recently provided evidence that cardiac sodium channels ($Na_v1.5$) within the perinexus, a specialized nanodomain of non-junctional membrane surrounding Cx43 GJ, play a major role in the propagation of electrical excitation in the heart via ephaptic mechanisms.(34) In this study, we demonstrate that $K_{ir}2.1$ is enriched along with $Na_v1.5$ in this same nanodomain. Further, we provide evidence that partially inhibiting $K_{ir}2.1$ channels increases conduction velocity under control conditions,(35) as well as during AIE, provided that I_{Na} is not also inhibited. Aside from highlighting I_{K1} inhibition as a strategy to mitigate arrhythmogenic conduction slowing during AIE, these data suggest that ID-localized potassium channels may be important modulators of ephaptic coupling between myocytes.

Previously, we proposed that close membrane apposition (up to 20 or 30 nm) and enrichment of cardiac sodium channels ($Na_v1.5$) within the perinexus allow the perinexus to function as a cardiac ephapse between ventricular myocytes,(34) which is consistent with

theoretical predictions from multiple investigators.(12, 16, 21, 28) In our previous study, using gSTED imaging, we demonstrated that $Na_v1.5$ clusters occurred within the perinexal regions of over half of Cx43 GJs identified in guinea pig ventricles.(34) In a more recent study, we reported a median distance of 71 ± 33 nm from Cx43 clusters to the nearest $Na_V1.5$ clusters in adult guinea pig ventricles as quantified by STORM-RLA, i.e. 50% of GJ had $Na_V1.5$ located less than 71 nm away, well within their perinexi.(32) Here, we demonstrate in neonatal rat ventricular myocytes that a near-identical 53% of GJ had $Na_v1.5$ within their perinexi.

While ventricular myocytes show important differences in the organization of the molecular components of electrical excitation between different species and at different developmental stages, the similarities in perinexal enrichment of $Na_v1.5$ and $K_{ir}2.1$ adjacent to Cx43 GJ in both the adult guinea pig and the immature rat heart suggest high levels of conservation in the ultrastructure of this nanodomain. Interestingly, $Na_v1.5$ was also reported to be enriched adjacent to desmosomes,(1) however, intermembrane spacing at these locations exceeds 50 nm.(15) Given that computer models stipulate intermembrane distance <=30nm for ephaptic coupling to occur, the perinexal ion channels may represent a specialized sub-population even within ID, capable of modulating ephaptic coupling. Therefore, these data underscore the importance of ultrastructural organization of ion channels within the ID for cardiac conduction.

We previously demonstrated that partial $K_{ir}2.1$ inhibition alone increases CV during control conditions.(35) Here we evaluated conduction dependence on $K_{ir}2.1$ when ephaptic coupling is compromised secondary to increased perinexal membrane spacing during mannitol-induced AIE.(34, 36) Interestingly, $K_{ir}2.1$ inhibition during AIE preferentially increased CV_T relative to AIE alone. This is consistent with our previous report that inhibiting another channel found in the perinexus ($Na_v1.5$) can preferentially slow CV_T during AIE. To elaborate, if ion channels located within intercalated disc nanodomains, such as the perinexus, are involved in intercellular communication, then it would be anticipated that an activation wavefront traveling transverse to the fiber axis would encounter more disc-localized GJ and associated perinexi per unit distance traveled than a wavefront traveling along the fiber axis. Thus, the observation that CV_T was preferentially altered by modulating $Na_v1.5$ and $K_{ir}2.1$ channels during AIE, supports a role for these channels in intercellular coupling. While $K_{ir}2.1$ modulation has been previously demonstrated to modulate conduction velocity,(20, 35) to our knowledge, this is the first demonstration that I_{K1} can anisotropically modulate conduction during AIE.

In addition to $Na_v1.5$ and $K_{ir}2.1$, previous studies have reported preferential localization of $K_V1.5$,(19) the voltage-gated, shaker-related potassium channel, small conductance calcium-activated potassium (SK) channels(26), and $K_{ir}6.2$, the ATP-sensitive potassium channel,(9) at the intercalated disc. Also, we have demonstrated that activation of the rapid (HERG)(14) and slow (KvLQT1)(33) delayed rectifier potassium channels as well as $K_{ir}6.2$ can modulate cardiac conduction. Determining which of these channels, if any, also associate with the perinexus will be a useful avenue of inquiry. If more channels are identified within the perinexus, it would suggest that the narrow region of membrane at the edge of GJs contains multi-component complexes of ion channels associated with cardiac excitation. Thus, these

structures may represent molecular machinery central to intercellular propagation in the heart.

We demonstrated in an earlier study that modulating I_{K1} could not rescue conduction when I_{Na} was inhibited.(35) Our observation here that I_{K1} inhibition did not significantly affect CV during a combination of AIE and I_{Na} inhibition is consistent with these earlier results. Overall, the finding that AIE + I_{K1} inhibition reduced AR and VT incidence to levels not significantly different from control supports the hypothesis that preventing anisotropic conduction slowing is anti-arrhythmic.(3, 11) The inability of I_{K1} inhibition to increase CV during AIE + I_{Na} inhibition further underscores the central roles of $Na_v1.5$ and perinexal width to ephaptic coupling. Importantly, this study suggests that when a single theoretical determinant of ephaptic coupling is reduced (eg. increased perinexal width), then relatively smaller currents like I_{K1} can significantly modulate conduction. Consistent with double hit hypothesis, i.e. the idea that compromise of multiple determinants of conduction results in a more severe phenotype,(18, 29, 30) we find a diminished role for smaller currents like I_{K1} in rescuing ephaptic coupling when multiple determinants of ephaptic coupling are simultaneously reduced. Finally, the idea that multiple determinants of cardiac conduction must be simultaneously altered in order to observe conduction slowing has been suggested as the basis of the “Conduction Reserve” hypothesis.(29) We propose that ephaptic coupling may be a principal determinant of conduction reserve.

In earlier studies, we previously proposed the mechanism by which I_{K1} modulates conduction is by opposing I_{Na} depolarization very early in the action potential.(35) Our results herein support a similar mechanism operating locally within the perinexal ephapse whereby efflux of K^+ into the perinexal extracellular cleft opposes the local potential change precipitated by the withdrawal of Na^+ by $Na_v1.5$ channels. Thus, $K_{ir}2.1$ channels may constitute an opposing force to ephaptic coupling in much the same way as they oppose membrane depolarization in other parts of the myocyte membrane. However, this hypothesis does not preclude the possibility that $K_{ir}2.1$ localization within intercalated disc nanodomains may result in a different local resting membrane potentials within these pockets relative to the lateral sarcolemma. It is important to note that $K_{ir}6.2$ is also located at the intercalated disc and around the sarcolemma.(9) Therefore, the localization-dependent role of potassium channels as direct determinants of cardiac conduction merits further investigation.

While previous mathematical models have suggested that $Na_v1.5$ localization to the intercalated disc can modulate ephaptic coupling by electric fields,(12, 16, 21, 28) the proposal that potassium channel localization to these same nanodomains may modulate ephaptic communication is novel. Importantly, the mathematical modeling results highlight the functional implications of sodium and potassium channel enrichment at the intercalated disc: The *polarized model* but not the *uniform model* was able to correctly predict the experimentally observed preferential response of CV_T to I_{K1} and I_{Na} modulation during AIE. Furthermore, a purely electrotonic view of cardiac conduction anticipates that modulating an ionic current should affect excitability but not intercellular coupling; therefore, it should affect CV isotropically.(11) Yet, our experimental data show that modulating I_{Na} or I_{K1} during AIE anisotropically alters conduction in a manner consistent

with altered intercellular communication. It is also notable that the *polarized model* incorporating sodium and potassium channel enrichment at cell-cell contacts and ephaptic coupling well predicts experimentally observed behavior across six different experimental conditions. Therefore, our results suggest that K^+ channels can modulate anisotropic conduction and that their localization to specific nanodomains of the myocyte membrane may be a key determinant of their role in cardiac conduction.

Limitations

Although our polarized model includes the enrichment of $Na_v1.5$ and $K_{ir}2.1$ at the intercalated disc, it does not incorporate the full structural complexity of the intercalated disc as observed using electron microscopy.(5, 8, 10) Thus, nanodomain ion accumulation / depletion events, which are key to ephaptic coupling, are only approximated by the model. Additionally, pharmacological agents used in experimental studies have off-target effects: Although flecainide is a potent I_{Na} blocker, it has been shown to inhibit the transient outward potassium current (I_{to}) and a maintained outward potassium current (I_K) in rat.(27) Similarly, $BaCl_2$ has some cross-reactivity with the L-type calcium channel,(4) albeit at concentrations far greater than used in this study. The hypothesis forwarded in this manuscript does not preclude a role for protein remodeling in modulating conduction under these conditions. However, the study demonstrates that $K_{ir}2.1$ enrichment at the intercalated disc is important for computational models of ephaptic coupling.

Conclusion

Anisotropic conduction slowing is strongly correlated to the risk of conduction block leading to ventricular arrhythmias. Previously, the major determinants of anisotropic conduction were theorized to be myocyte size and gap junction coupling. A growing body of evidence, including the data provided herein, supports the hypothesis that ion channels localized to intercalated disc nanodomains such as the perinexus may also play a role in electrically coupling myocytes and thus, emerge as determinants of anisotropic conduction. While these data have yet to be validated in larger vertebrates, and particularly humans, the findings suggest that preserving ephaptic coupling mechanisms may be as viable an anti-arrhythmic target as modulating gap junctions.

Acknowledgments

The authors would like to thank Dr. James Smyth for assistance with STORM microscopy. Thanks also to Dr. Gregory Hoeker and Michael Entz for assistance with optical mapping experiments and to Mrs. Jane Jourdan for assistance with NRVM experiments.

Funding Sources: This work was supported by an NIH R01 grant awarded to Dr. Poelzing (R01-HL102298-01A1), an NIH R01 grant awarded to Dr. Gourdie (RO1 HL56728-14A2) and by an American Heart Association post-doctoral fellowship awarded to Dr. Veeraraghavan (2013-15; completed).

References

1. Agullo-Pascual E, Lin X, Leo-Macias A, Zhang M, Liang FX, Li Z, Pfenniger A, Lubkemeier I, Keegan S, Fenyo D, Willecke K, Rothenberg E, Delmar M. Super-resolution imaging reveals that loss of the C-terminus of connexin43 limits microtubule plus-end capture and NaV1.5 localization at the intercalated disc. Cardiovascular research. 2014

2. Clausen Mathias P, Galiani S, de la Serna Jorge B, Fritzsche M, Chojnacki J, Gehmlich K, Lagerholm BC, Eggeling C. Pathways to optical STED microscopy. NanoBioImaging. 2013:1.

3. Dhein S, Seidel T, Salameh A, Jozwiak J, Hagen A, Kostelka M, Hindricks G, Mohr FW. Remodeling of cardiac passive electrical properties and susceptibility to ventricular and atrial arrhythmias. Front Physiol. 2014; 5:424. [PubMed: 25404918]

4. Ferreira G, Yi J, Rios E, Shirokov R. Ion-dependent inactivation of barium current through L-type calcium channels. The Journal of general physiology. 1997; 109:449–461. [PubMed: 9101404]

5. Geisler SB, Green KJ, Isom LL, Meshinchi S, Martens JR, Delmar M, Russell MW. Ordered assembly of the adhesive and electrochemical connections within newly formed intercalated disks in primary cultures of adult rat cardiomyocytes. Journal of biomedicine & biotechnology. 2010; 2010:624719. [PubMed: 20467587]

6. George SA, Sciuto KJ, Lin J, Salama ME, Keener JP, Gourdie RG, Poelzing S. Extracellular sodium and potassium levels modulate cardiac conduction in mice heterozygous null for the Connexin43 gene. Pflugers Arch. 2015

7. Girouard SD, Laurita KR, Rosenbaum DS. Unique properties of cardiac action potentials recorded with voltage-sensitive dyes. Journal of cardiovascular electrophysiology. 1996; 7:1024–1038. [PubMed: 8930734]

8. Green CR, Severs NJ. Gap junction connexon configuration in rapidly frozen myocardium and isolated intercalated disks. The Journal of cell biology. 1984; 99:453–463. [PubMed: 6086670]

9. Hong M, Bao L, Kefaloyianni E, Agullo-Pascual E, Chkourko H, Foster M, Taskin E, Zhandre M, Reid DA, Rothenberg E, Delmar M, Coetzee WA. Heterogeneity of ATP-sensitive K+ channels in cardiac myocytes: enrichment at the intercalated disk. The Journal of biological chemistry. 2012; 287:41258–41267. [PubMed: 23066018]

10. Hoyt RH, Cohen ML, Saffitz JE. Distribution and three-dimensional structure of intercellular junctions in canine myocardium. Circulation research. 1989; 64:563–574. [PubMed: 2645060]

11. Kleber AG, Rudy Y. Basic mechanisms of cardiac impulse propagation and associated arrhythmias. Physiological reviews. 2004; 84:431–488. [PubMed: 15044680]

12. Kucera JP, Kleber AG, Rohr S. Slow conduction in cardiac tissue, II: effects of branching tissue geometry. Circulation research. 1998; 83:795–805. [PubMed: 9776726]

13. Kucera JP, Rohr S, Rudy Y. Localization of sodium channels in intercalated disks modulates cardiac conduction. Circulation research. 2002; 91:1176–1182. [PubMed: 12480819]

14. Larsen AP, Olesen SP, Grunnet M, Poelzing S. Pharmacological activation of IKr impairs conduction in guinea pig hearts. Journal of cardiovascular electrophysiology. 2010; 21:923–929. [PubMed: 20163495]

15. Leo-Macias A, Liang FX, Delmar M. Ultrastructure of the intercellular space in adult murine ventricle revealed by quantitative tomographic electron microscopy. Cardiovascular research. 2015; 107:442–452. [PubMed: 26113266]

16. Lin J, Keener JP. Ephaptic coupling in cardiac myocytes. IEEE transactions on bio-medical engineering. 2013; 60:576–582. [PubMed: 23335235]

17. Lin J, Keener JP. Microdomain effects on transverse cardiac propagation. Biophysical journal. 2014; 106:925–931. [PubMed: 24559995]

18. Matthes S, Zhang M, Taffet S, Delmar M. Desmosomes and Gap Junctions in Epicardium-Derived Cells. A Possible Role in Arrhythmogenic Right Ventricular Cardiomyopathy? Heart rhythm : the official journal of the Heart Rhythm Society. 2010; 7:1715–1716.

19. Mays DJ, Foose JM, Philipson LH, Tamkun MM. Localization of the Kv1.5 K+ channel protein in explanted cardiac tissue. The Journal of clinical investigation. 1995; 96:282–292. [PubMed: 7615797]

20. Milstein ML, Musa H, Balbuena DP, Anumonwo JM, Auerbach DS, Furspan PB, Hou L, Hu B, Schumacher SM, Vaidyanathan R, Martens JR, Jalife J. Dynamic reciprocity of sodium and potassium channel expression in a macromolecular complex controls cardiac excitability and arrhythmia. Proceedings of the National Academy of Sciences of the United States of America. 2012; 109:E2134–2143. [PubMed: 22509027]

21. Mori Y, Fishman GI, Peskin CS. Ephaptic conduction in a cardiac strand model with 3D electrodiffusion. Proceedings of the National Academy of Sciences of the United States of America. 2008; 105:6463–6468. [PubMed: 18434544]
22. Poelzing S, Veeraraghavan R. Heterogeneous ventricular chamber response to hypokalemia and inward rectifier potassium channel blockade underlies bifurcated T wave in guinea pig. American journal of physiology Heart and circulatory physiology. 2007; 292:H3043–3051. [PubMed: 17307991]
23. Rhett JM, Jourdan J, Gourdie RG. Connexin 43 connexon to gap junction transition is regulated by zonula occludens-1. Molecular biology of the cell. 2011; 22:1516–1528. [PubMed: 21411628]
24. Rhett JM, Ongstad EL, Jourdan J, Gourdie RG. Cx43 Associates with Na(v)1.5 in the Cardiomyocyte Perinexus. The Journal of membrane biology. 2012; 245:411–422. [PubMed: 22811280]
25. Schoonderwoert V, Dijkstra R, Luckinavicius G, Kobler O, van der Voort H. Huygens STED Deconvolution Increases Signal-to-Noise and Image Resolution towards 22 nm. Microscopy Today. 2013; 21:38–44.
26. Skibsbye L, Wang X, Axelsen LN, Bomholtz SH, Nielsen MS, Grunnet M, Bentzen BH, Jespersen T. Antiarrhythmic Mechanisms of SK Channel Inhibition in the Rat Atrium. Journal of cardiovascular pharmacology. 2015; 66:165–176. [PubMed: 25856531]
27. Slawsky MT, Castle NA. K+ channel blocking actions of flecainide compared with those of propafenone and quinidine in adult rat ventricular myocytes. The Journal of pharmacology and experimental therapeutics. 1994; 269:66–74. [PubMed: 8169853]
28. Sperelakis N, McConnell K. Electric field interactions between closely abutting excitable cells. IEEE engineering in medicine and biology magazine : the quarterly magazine of the Engineering in Medicine & Biology Society. 2002; 21:77–89.
29. Stein M, Boulaksil M, Engelen MA, van Veen TA, Hauer RN, de Bakker JM, van Rijen HV. Conduction reserve and arrhythmias. Neth Heart J. 2006; 14:113–116. [PubMed: 25696607]
30. Stein M, van Veen TA, Remme CA, Boulaksil M, Noorman M, van Stuijvenberg L, van der Nagel R, Bezzina CR, Hauer RN, de Bakker JM, van Rijen HV. Combined reduction of intercellular coupling and membrane excitability differentially affects transverse and longitudinal cardiac conduction. Cardiovascular research. 2009; 83:52–60. [PubMed: 19389723]
31. Tran TN, Drab K, Daszykowski M. Revised DBSCAN algorithm to cluster data with dense adjacent clusters. Chemometrics and Intelligent Laboratory Systems. 2013; 120:92–96.
32. Veeraraghavan R, Gourdie R. Stochastic Optical Reconstruction Microscopy-based Relative Localization Analysis (STORM-RLA) for Quantitative Nanoscale Assessment of Spatial Protein Organization. Molecular biology of the cell. 2016
33. Veeraraghavan R, Larsen AP, Torres NS, Grunnet M, Poelzing S. Potassium channel activators differentially modulate the effect of sodium channel blockade on cardiac conduction. Acta Physiol (Oxf). 2013; 207:280–289. [PubMed: 22913299]
34. Veeraraghavan R, Lin J, Hoeker GS, Keener JP, Gourdie RG, Poelzing S. Sodium channels in the Cx43 gap junction perinexus may constitute a cardiac ephapse: an experimental and modeling study. Pflugers Arch. 2015
35. Veeraraghavan R, Poelzing S. Mechanisms Underlying Increased Right Ventricular Conduction Sensitivity to Flecainide Challenge. Cardiovascular research. 2008; 77:749–756. [PubMed: 18056761]
36. Veeraraghavan R, Salama ME, Poelzing S. Interstitial Volume Modulates the Conduction Velocity-Gap Junction Relationship. American journal of physiology Heart and circulatory physiology. 2012

Significance

For over half a century, electrical excitation in the heart has been thought to occur exclusively via gap junction-mediated ionic current flow between cells. Further, excitation was thought to depend almost exclusively on sodium channels with potassium channels being involved mainly in returning the cell to rest. Here, we demonstrate that sodium and potassium channels co-reside within nano-scale domains at cell-to-cell contact sites. Experimental and computer modeling results suggest a role for these channels in electrical coupling between cardiac muscle cells via an ephaptic mechanism working in tandem with gap junctions. This new insight into the mechanism of cardiac electrical excitation could pave the way for novel therapies against cardiac rhythm disturbances.

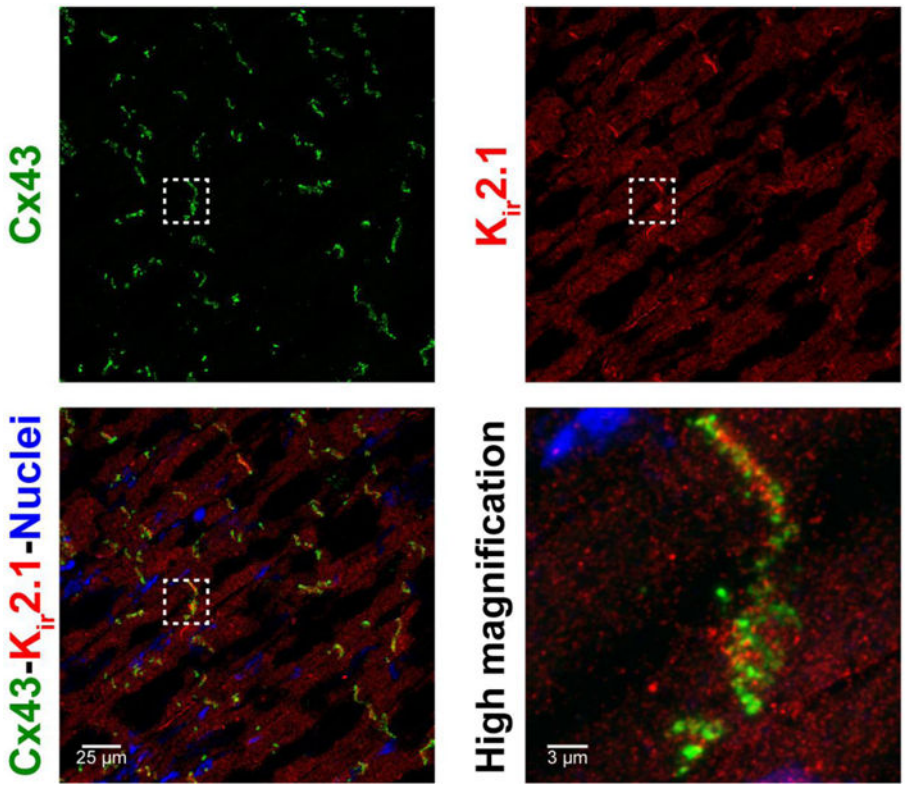

Figure 1. K_{ir}2.1 at the ID

Representative confocal images of **A)** Cx43, **B)** K_{ir}2.1 and **C)** overlay demonstrate co-localization of Cx43 and K_{ir}2.1 in ventricular sections. **D)** A close up view demonstrates enrichment of Cx43 and K_{ir}2.1 at the ID.

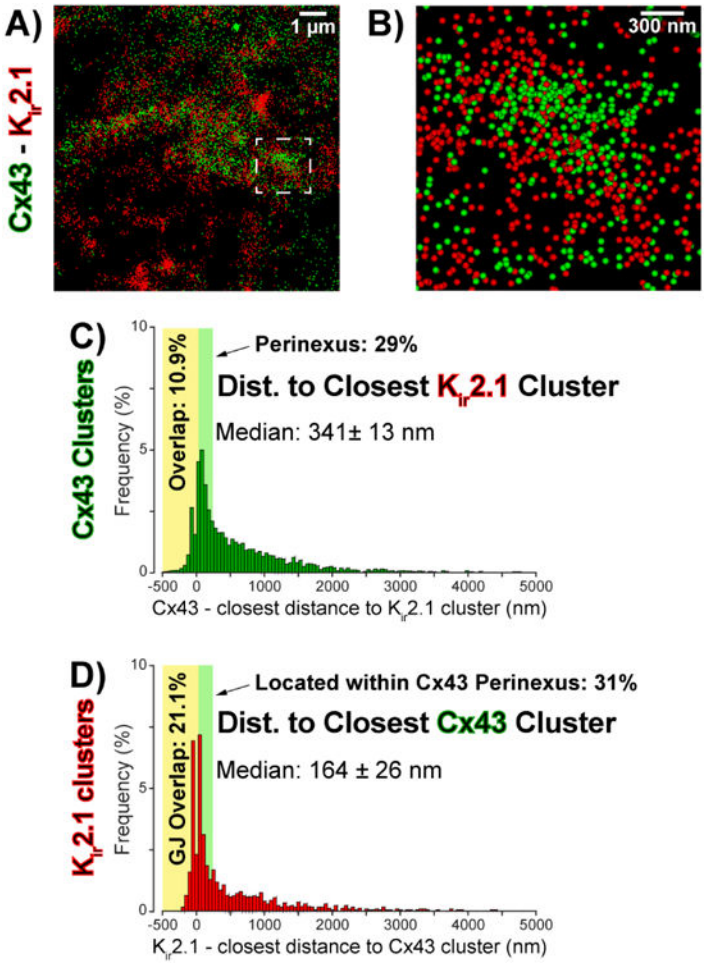

Figure 2. Cx43 and $K_{ir}2.1$ relative localization

A) Representative STORM micrograph of an ID from guinea pig ventricles showing Cx43 (green) and $K_{ir}2.1$ (red) immunosignals. **B)** A high magnification view of the region highlighted by the dashed white box in A. **C)** Edge-to-edge distance from Cx43 clusters to the closest $K_{ir}2.1$ cluster. **D)** Edge-to-edge distance from $K_{ir}2.1$ clusters to the closest Cx43 cluster.

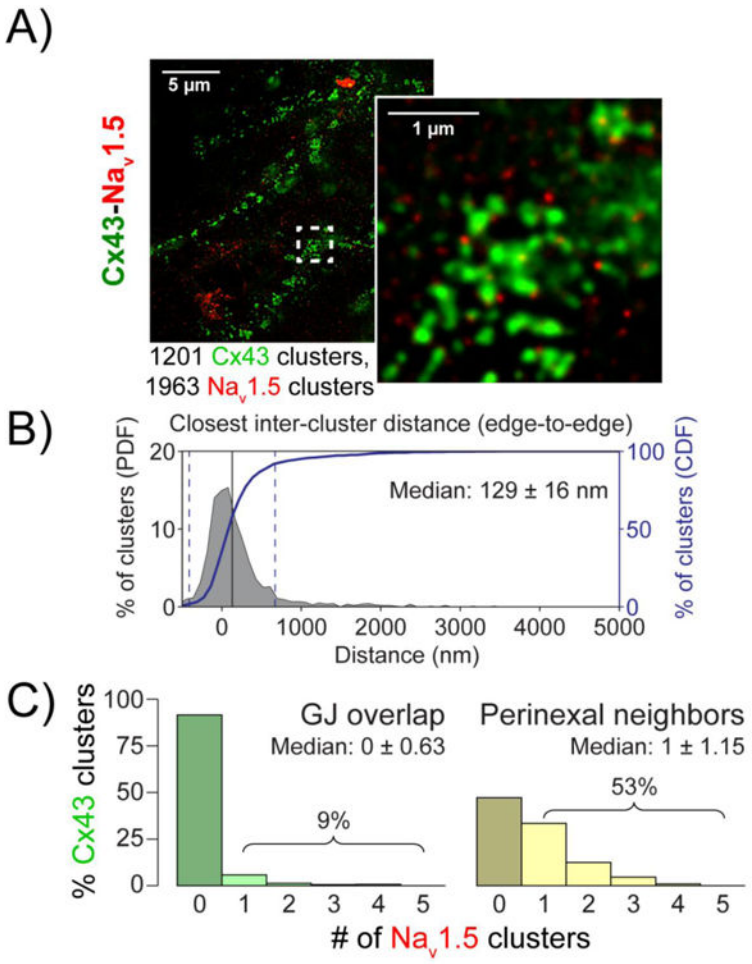

Figure 3. Cx43 and Na$_v$1.5 relative localization

A) Representative gSTED micrograph of NRVMs showing Cx43 (green) and Na$_v$1.5 (red) immunosignals. Inset shows high magnification view of the region highlighted by the dashed white box. **B)** Edge-to-edge distance from Cx43 clusters to the closest Na$_v$1.5 cluster. **C)** Histograms of Cx43 clusters by number of Na$_v$1.5 clusters demonstrating direct overlap (left, green) and located within the perinexus (right, yellow).

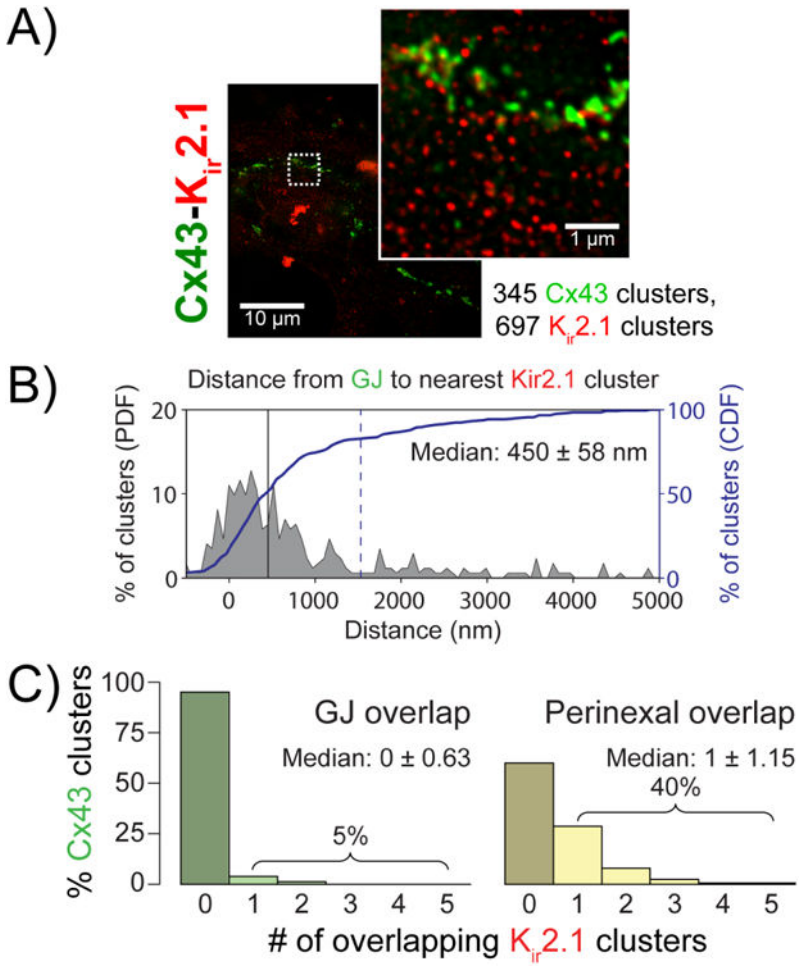

Figure 4. Cx43 and K_{ir}2.1 relative localization

A) Representative gSTED micrograph of NRVMs showing Cx43 (green) and K_{ir}2.1 (red) immunosignals. Inset shows high magnification view of the region highlighted by the dashed white box. **B)** Edge-to-edge from Cx43 clusters to the closest K_{ir}2.1 cluster. **C)** Histograms of Cx43 clusters by number of K_{ir}2.1 clusters demonstrating direct overlap (left, green) and located within the perinexus (right, yellow).

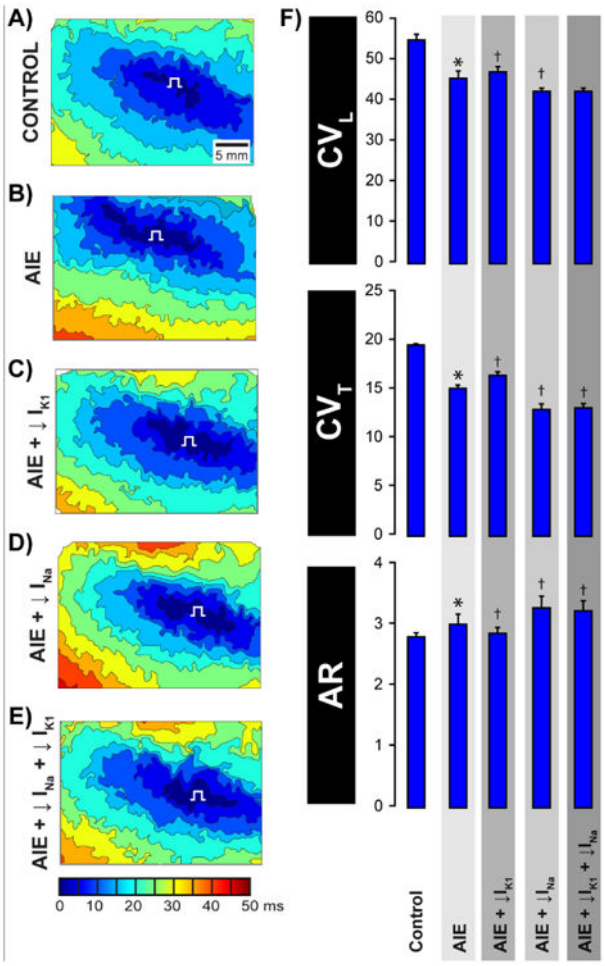

Figure 5. Inhibiting $K_{ir}2.1$ channels mitigates AIE-induced conduction slowing

Representative activation isochrones maps during **A)** Control, **B)** AIE, **C)** AIE + I_{K1} inhibition, **D)** AIE + I_{Na} inhibition and **E)** AIE + I_{Na} inhibition + I_{K1} inhibition. **F)** Summary bar graphs of CV_L, CV_T and AR. n=5 hearts/group, * $p<0.05$ vs. control, † $p<0.05$ vs. AIE.

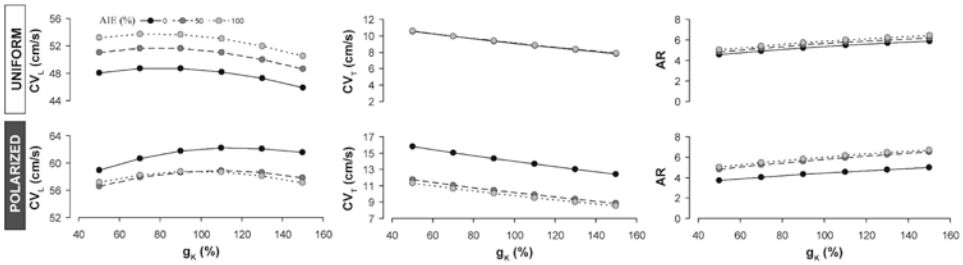

Figure 6. Modeling results: Conduction dependence on potassium conductance

Predictions of CV_L, CV_T and AR as a function of g_K at different levels of σ_e generated by the *uniform model* (top) and the *polarized model* (bottom).

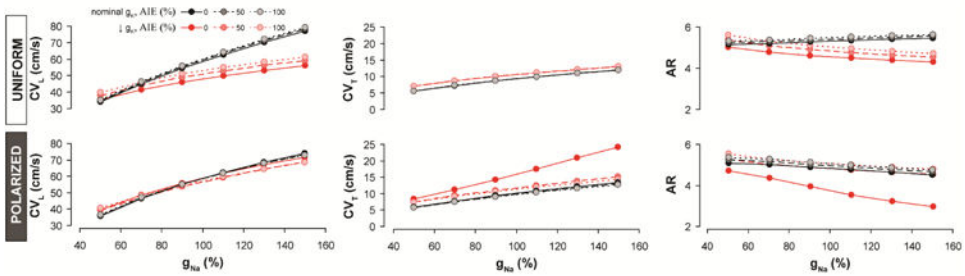

Figure 7. Modeling results: Conduction dependence on sodium conductance

Predictions of CV_L, CV_T and AR as a function of g_{Na} at different levels of σ_e under normal (black) and reduced (red) g_K generated by the *uniform model* (top) and the *polarized model* (bottom).

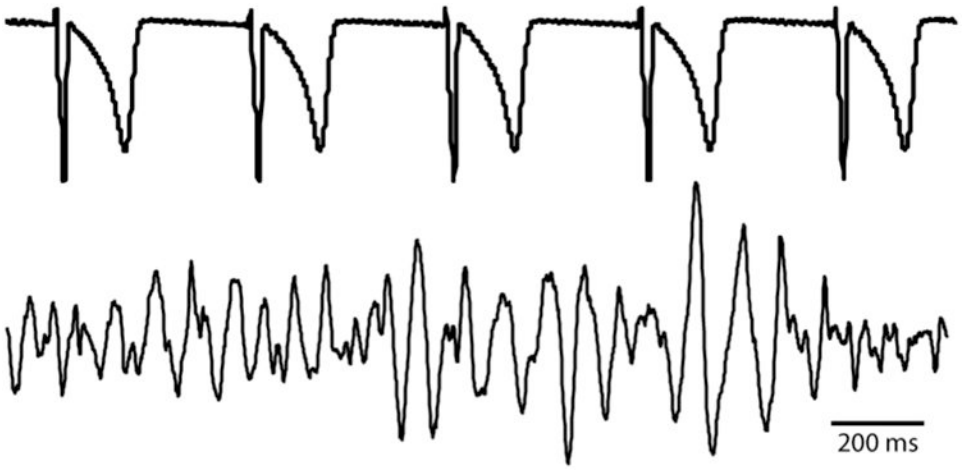

Figure 8. Volume-conducted ECGs: VT's during AIE

The top trace shows a sample volume-conducted ECG trace of intrinsic rhythm during AIE which had a cycle length of 408 ms. The bottom trace shows a representative ventricular tachyarrhythmia during AIE which had an average cycle length of 70 ms.

Table 1

Nanodomain model parameters

Structural parameters:		
Cell length		101 μm
Cell width		24.1 μm
Cellular offset		50% transverse, 20% longitudinal
Junctional sodium current density		11 to 90% of total
Junctional potassium current density		11 to 90% of total
Nominal Conductances:		
GJ coupling		$\bar{g}_j$ = 100 mS/cm^2
Extracellular width - junctional		15 nm
Extracellular width - lateral		0.1 μm
Lateral extracellular conductivity ($\bar{\sigma}_e$)		159.1 mS/cm
Junctional extracellular conductivity ($\bar{\sigma}_j$)		17.8 mS/cm
Interventions:		
AIE	$\bar{\sigma}_e$	203.5 mS/cm
	$\bar{\sigma}_j$	62.8 mS/cm